ACS Catalysis

RESEARCH ARTICLE

pubs.acs.org/acscatalysis

Active Sites for the Reaction of Ethanol to Acetaldehyde on Co/YSZ(100) Model Steam Reforming Catalysts

Eddie Martono and John M. Vohs*

Department of Chemical and Biomolecular Engineering, University of Pennsylvania, Philadelphia, Pennsylvania 19104, United States

ABSTRACT: Structure−activity relationships for the reaction of ethanol on model Co/YSZ(100) (YSZ = yttria-stabilized ZrO_2) steam reforming catalysts were investigated using temperature-programmed desorption (TPD) and X-ray photoelectron spectroscopy and compared with those obtained previously for the reaction of ethanol on Co/ZnO(0001) and Co foils. Oxygen-free, metallic Co sites were found to be active for ethanol decarbonylation to form CO, H_2, and adsorbed CH_3 groups, whereas oxygen adatoms on metallic Co promoted ethoxide dehydrogenation to produce acetaldehyde at 330 K during TPD. In contrast, oxidized Co surfaces containing only Co^{2+} sites were found to be less reactive for ethanol dehydrogenation producing acetaldehyde at 480 K. These results, along with comparisons with those from Co/ZnO(0001) and Co foils, provide new insights into the active sites for ethanol steam reforming on Co-based catalysts and the influence of the support on both catalyst reactivity and stability.

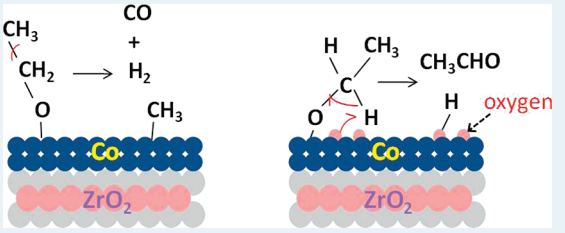

KEYWORDS: ethanol, steam reforming, cobalt, zirconia, acetaldehyde, reducible support, surface oxygen

INTRODUCTION

Currently, we rely heavily on the use of nonrenewable energy sources, such as fossil fuels. The dwindling reserves of these fuels and the fact that their utilization results in the release of greenhouse gases has motivated the development of more renewable energy sources and highly efficient methods for their conversion. Hydrogen-powered fuel cells is one technology that has received much attention[1,2] in this regard. For this approach to have an impact, however, efficient methods to produce H_2, preferably from biorenewable sources, is required. Producing H_2 via the steam reforming of ethanol ($C_2H_5OH + 3H_2O \rightarrow 6H_2 + 2CO_2$) is one approach to addressing this issue, since ethanol can be derived from a range of biomass-derived sources and has the added advantages of low toxicity and being relatively easy to store and transport. This interest in ethanol as a potential biorenewable H_2 source has, in turn, motivated research into highly active and selective ethanol steam reforming catalysts.[3−8]

Precious metal catalysts (i.e., Rh and Pd) have been reported to be highly active for the steam reforming of ethanol (SRE),[9−11] but the high cost of these materials is a major drawback that limits their large-scale application. Recently, Co-based catalysts have emerged as an alternative, with reported activity that is comparable to that of the precious metals.[8,12] For example, some reports indicate that Co catalysts can achieve SRE selectivities to CO_2 and H_2 in excess of 90% at relatively low temperatures with CH_4, CH_3CHO, C_2H_4, and $(CH_3)_2CO$ being the primary side products.[8] The selectivity is highly dependent on the structure of the catalyst, however, and it has been shown that the support plays a major role in influencing the overall activity and product distribution. A survey of previous studies of Co-based SRE catalysts indicates that reducible supports, such as ZnO and CeO_2, generally produce more selective catalysts compared with more refractory supports, such as Al_2O_3, MgO, and ZrO_2.[8,13−16] Reducible supports also appear to produce catalysts that are less prone to deactivation via carbon buildup on the metal.[17,18] The mechanism by which the support affects reactivity has yet to be completely determined. Another important aspect of these catalysts that has yet to be resolved concerns the active form of the cobalt. Several studies have concluded that metallic cobalt is required,[15,19] while others indicate the need for both metallic and oxidized cobalt.[20−22]

To provide a better understanding of the active sites and the role of metal−support interactions in cobalt-based catalysts for ethanol steam reforming, we have previously studied the interfacial chemistry and ethanol reactivity on model Co catalysts consisting of polycrystalline cobalt foils and cobalt films and particles supported on ZnO(0001).[23−25] Much of this work focused on identifying the active sites for the dehydrogenation of adsorbed ethoxide intermediates to produce acetaldehyde, since this is thought to be a key step in achieving high selectivities to H_2 and CO_2 during SRE.[13,18,20,26−28] Our studies show that on oxygen-free, metallic cobalt surfaces, ethoxide species undergo decarbonylation to produce CO and adsorbed methyl groups. In contrast, on Co surfaces that are partially covered with oxygen or contain a mixture of Co^0 and Co^{2+} sites, dehydrogenation of adsorbed ethoxide intermediates to produce acetaldehyde proceeds with a relatively low activation energy.[24,25] For Co/ZnO(0001), facile exchange of oxygen between the ZnO and the Co appears to facilitate this reaction.[22] Whether Co^{2+} sites or merely oxygen adatoms on metallic Co are required is still an open question. In the work reported here, we have expanded these studies to include the reaction of ethanol on Co supported

Received: August 3, 2011
Revised: September 10, 2011
Published: September 12, 2011

on the (100) surface of an yttria-stabilized, ZrO_2 single crystal (YSZ(100)). Zirconia was chosen as a prototypical, nonreducible support. The results of this study along with comparisons with our previous data for the reactivity of Co on the more reducible ZnO(0001) support provide new insight into the active sites for ethanol steam reforming and the role of the support in determining catalytic activity and stability.

EXPERIMENTAL METHODS

All experiments were carried out in an ultrahigh vacuum (UHV) surface analysis chamber with a background pressure of 2×10^{-10} Torr. This chamber was equipped with an ion sputter gun (Physical Electronics) for sample cleaning, a quadrupole mass spectrometer (UTI) for temperature-programmed desorption (TPD) studies, and a hemispherical electron energy analyzer (Leybold-Heraeus) and X-ray source (VG Microtech).

A $6 \times 6 \times 1$ mm YSZ(100) single crystal (MTI Corporation) was used as the support in this study. Yttria (8 mol %) was added to the crystal to stabilize the cubic zirconia phase, which has a fluorite structure. The YSZ(100) sample was mounted in a tantalum foil holder that was attached to the sample manipulator of the UHV chamber. Heating of the sample was achieved via conduction from the resistively heated tantalum holder, and the temperature was monitored using a chromel-alumel type K thermocouple that was attached to the back surface of the sample using a ceramic adhesive (Aremco). The YSZ(100) surface was cleaned by sputtering with 2 kV argon ions for 30 min, followed by annealing at 750 K for 1 h. This sputter/anneal cycle was repeated until the absence of impurities, such as carbon, was confirmed by X-ray photoelectron spectroscopy (XPS).

Co was deposited using an electron beam evaporator (Tetra GmbH) with a 2 mm diameter Co rod (Alfa Aesar, 99.995% purity) source. The flux of Co was monitored using a quartz crystal film thickness monitor (Q-pod, Inficon). The deposition of Co was conducted with the YSZ(100) substrate at 300 K with a growth rate of ~0.1 A/s. In this paper, the Co coverage is reported in monolayers (ML), where one monolayer is defined to have 1.8×10^{15} atoms/cm^2 which is equal to the atom density on Co(0001).

Ethanol (Decon Laboratories, Inc., 100%) and oxygen (Matheson, 99.98%) were introduced into the UHV chamber through a variable leak valve with the sample positioned directly in front of a dosing needle. The enhancement factor of 100-fold due to direct dosing was used and factored into all doses reported. A 2 L ethanol dose with the sample maintained at 298 K was used in each TPD experiment, except where specified otherwise. This dose was found to be sufficient to saturate the surface with ethanol. Since the Co metal source outgases some CO and H_2O when in operation, freshly prepared Co/YSZ(100) samples were flashed to 500 K prior to any TPD experiments to remove these impurities from the surface. As will be discussed below, this treatment does not result in any significant changes in the structure of the Co film or the Co oxidation state. The TPD experiments were performed with a heating rate of 3 K/s.

RESULTS

Characterization of Co Film Growth. Figure 1 shows the Co(2p) XP spectra as a function of the nominal Co coverage on the YSZ(100) substrate for Co deposition at 300 K. The intensity of ZrO_2 coming from the support was monitored from the

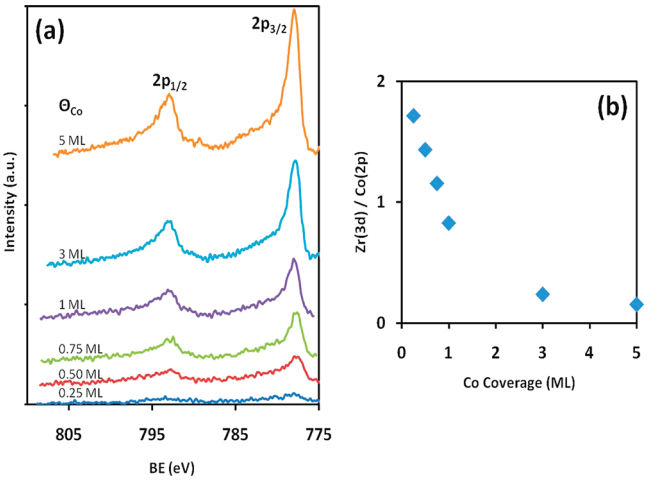

Figure 1. (a) Co(2p) XP-spectra and (b) Zr(3d)/Co(2p) peak area ratios as a function of the Co coverage on the YSZ(100) substrate.

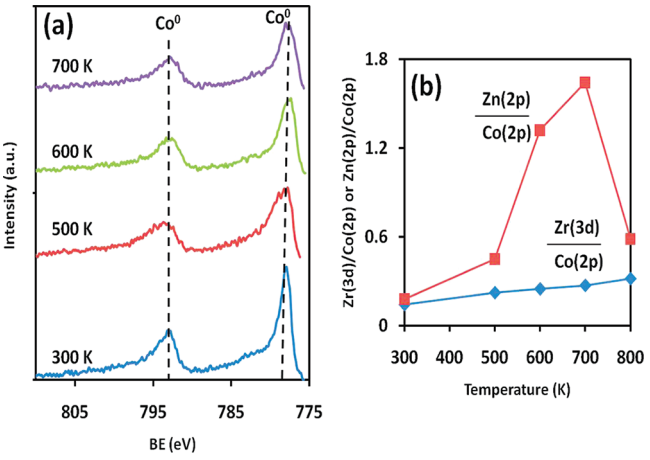

Figure 2. (a) XP-spectra of 2 ML Co/YSZ(100) sample as a function of the annealing temperature. (b) Zr(3d)/Co(2p) and Zn(2p)/Co(2p) peak area ratios as a function of the sample annealing temperature for 2 ML Co/YSZ(100) and 2 ML Co/ZnO(0001) samples.

existence of Zr $3d_{3/2}$ and $3d_{5/2}$ peaks located at 183.2 ± 0.2 and 185.6 ± 0.2 eV, respectively.[29,30] The ratio of the areas of the Zr(3d) and Co(2p) peaks as a function of Co coverage is also included in the figure. The Co(2p) peaks for all coverages indicate that the as-deposited Co existed primarily in the metallic state (Co^0), as determined from the sharp $2p_{3/2}$ and $2p_{1/2}$ peaks at 778.0 ± 0.2 and 793.0 ± 0.2 eV, respectively.[31,32] The steep, linear decrease in the Zr(3d)/Co(2p) ratio with increasing Co coverages up to 1 ML suggests that the Co film growth proceeds via the formation of two-dimensional islands rather three-dimensional clusters. This growth mechanism has also been reported for Pt on YSZ(100).[33,34]

The Co films on YSZ(100) were found to have relatively high thermal stability. This is demonstrated by the XPS data in Figure 2 for a 2 ML Co/YSZ(100) sample. Annealing the sample up to 800 K resulted in a small increase in the Zr(3d)/Co(2p) ratio, which is consistent with some agglomeration of the Co film into particles. For comparison purposes, the Zn(2p)-to-Co(2p) ratio as a function of temperature for a 2 ML Co film on a ZnO(0001) surface obtained in our previous study[25] is included

dx.doi.org/10.1021/cs200404h |ACS Catal. 2011, 1, 1414–1420

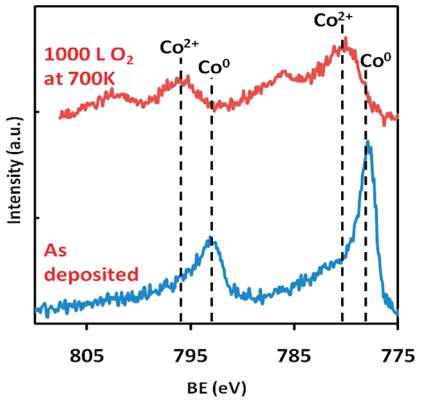

Figure 3. XP spectra of as-deposited 1 ML Co/YSZ(100) and after 1000 L O_2 exposure at 700 K.

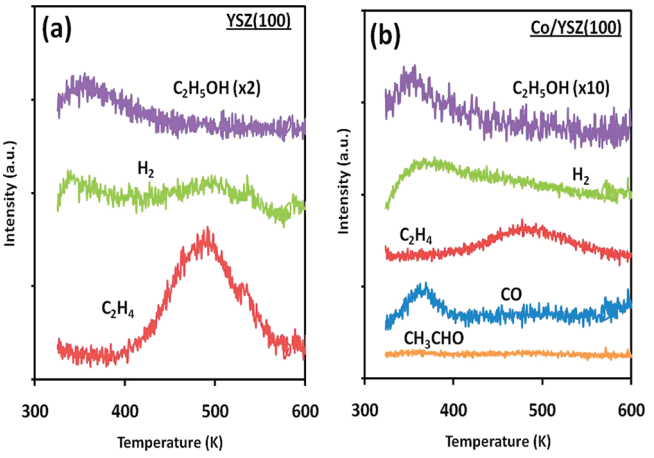

Figure 4. TPD obtained after a 2 L C_2H_5OH dose at 300 K on (a) YSZ(100) and (b) freshly deposited 1 ML Co/YSZ(100).

in the figure. On ZnO(0001), vapor-deposited Co also forms two-dimensional islands at 300 K. Note that in comparison with the results for Co/YSZ(100), the Zn(2p)/Co(2p) ratio increases much more abruptly when the sample is annealed above 500 K, indicating significant agglomeration of the Co film on the ZnO-(0001) surface. The sharp decrease upon heating to 800 K is due to the reaction of the Co with the ZnO to form CoO, which then spreads over the surface.[23,35] These results demonstrate that the interaction of metallic Co with zirconia is much stronger than that with ZnO, resulting in a more thermally stable film. This observation is in agreement with that reported by Padilla et al.[26] where high surface area Co/ZrO_2 catalysts were found to exhibit high thermal stability, suggesting a strong interaction between metal and support. Furthermore, Song et al.[13] report that cobalt supported on ZrO_2 maintains a higher metal dispersion as compared with TiO_2 or AlO_2 supports.

The XPS data in Figure 2 also show that the Co remained in the metallic state for annealing temperatures up to 700 K. This result is in contrast to that obtained for Co/ZnO(0001), in which, as noted above, oxidation of the Co to form CoO (i.e., Co^{2+}) occurred via a solid-state reaction with the ZnO lattice upon heating above 700 K. This oxidation reaction is partially responsible for the sharp decrease in the Zn(2p)/Co(2p) ratio after annealing to 800 K. CoO films on YSZ(100) could be produced,

Table 1. Relative Product Yields of Carbon-Containing Products during C_2H_5OH TPD

	Low Temp CO (360 K)	High Temp CO (518 K)	C_2H_4 (480 K)	CH_3CHO
Co/YSZ(100)	0.23		0.77	
CoO/YSZ(100)			0.50	0.5 (480 K)
O_2-dosed Co/YSZ(100)	0.16	0.12	0.16	0.56 (330 K)

however, by exposing the Co film to 1000 L of O_2 with the sample held at 700 K. This is demonstrated by the XPS data in Figure 3, which shows Co(2p) spectra for a 1 ML Co film before (A) and after (B) this oxidation treatment. Note the disappearance of the peaks corresponding to metallic Co and the emergence of the $2p_{3/2}$ and $2p_{1/2}$ peaks at 780.5 ± 0.5 and 796.0 ± 0.5 eV, respectively, indicative of Co^{2+}.[31,32,36,37]

TPD Reactivity Studies. Before presenting the data for the reaction of ethanol on Co/YSZ(100), it is useful to consider the reaction of ethanol on the clean YSZ(100) surface. Figure 4a shows TPD data obtained from a YSZ(100) sample dosed with 2 L of C_2H_5OH at 300 K. A small amount of molecular C_2H_5OH was observed to desorb broadly between 300 and 420 K. The only other products were C_2H_4 and H_2, which desorb at 485 K. Previous studies have shown that methanol adsorbs dissociatively on YSZ(100) to form adsorbed methoxide intermediates.[38] By analogy, ethanol would be expected to adsorb dissociatively to form ethoxide species on this surface. Thus, the C_2H_4 and H_2 products at 485 K can be attributed to a net dehydration reaction involving these ethoxide intermediates.

TPD spectra obtained following a 2 L dose of C_2H_5OH at 300 K on a 1 ML Co/YSZ(100) are shown in Figure 4b, and the product relative yields are listed in Table 1. As noted above, the freshly deposited Co film consists primarily of two-dimensional islands of Co^0. In addition to a small ethanol desorption peak at 320 K, the TPD spectra contain a broad H_2 desorption feature that extends from 320 K to above 500 K, a broad C_2H_4 peak at 480 K, and a much narrower CO desorption peak at 360 K. No other gaseous products, including acetaldehyde, were detected. On the basis of a comparison to the ethanol TPD data for the clean YSZ(100) surface, the C_2H_4 peak at 480 K can be attributed to the reaction of ethoxide species adsorbed on the YSZ. The presence of this peak also indicates that the vapor-deposited Co does not grow in a completely layer-by-layer fashion, since some of the YSZ(100) surface remains exposed for a 1 ML Co coverage.

The CO peak at 360 K was not present in the TPD spectra from the clean YSZ(100) surface and, therefore, must be due to the reaction of ethanol or ethoxide species adsorbed on the Co. This decarbonylation pathway would be expected also to produce adsorbed methyl groups. Since CO was the only gaseous carbon-containing product produced on the supported Co, the methyl groups must ultimately decompose, producing H_2 and depositing carbon on the surface. This is supported by the fact that in a C_2H_5OH TPD run obtained immediately after the one shown in Figure 4b, the CO peak resulting from the decarbonylation reaction on the metallic cobalt sites was nearly absent, suggesting that the Co sites are blocked by a surface carbon layer.

Additional support for the conclusion that carbon is deposited on the Co is provided by the TPD data in Figure 5, which displays CO and C_2H_4 desorption spectra obtained in three successive ethanol TPD experiments from a 3 ML Co/YSZ(100) sample.

dx.doi.org/10.1021/cs200404h |ACS Catal. 2011, 1, 1414–1420

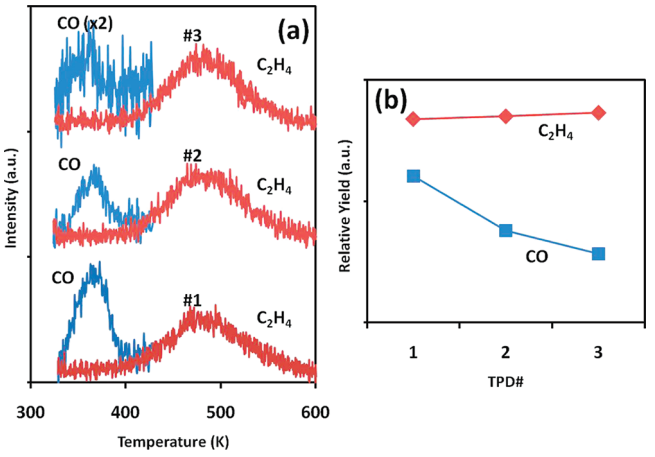

Figure 5. (a) CO and C_2H_4 desorption spectra obtained in a series of sequential TPD experiments with a 2 L C_2H_5OH-dosed, 3 ML Co/YSZ(100) sample. The run number for each experiment is indicated in the figure. (b) CO and C_2H_4 relative product yields for each C_2H_5OH TPD experiment.

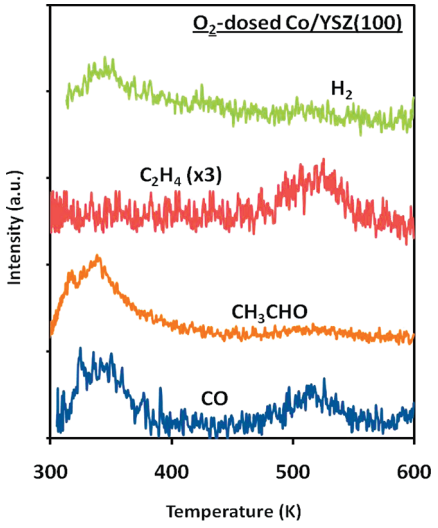

Figure 6. TPD spectra obtained following a 2 L C_2H_5OH dose at 300 K on a 1 L O_2 predosed Co/YSZ(100) sample.

A plot of the relative areas of the CO and C_2H_4 peaks as a function of the run number is also included in the figure. Note that the amount of CO produced via reaction of ethanol on the supported Co was found to decrease significantly with each successive experiment, whereas the amount of C_2H_4 remained nearly the same. The fact that the C_2H_4 peak due to reaction of ethanol on the exposed portions of the YSZ(100) surface was nearly invariant indicates that no significant agglomeration of the Co occurred during the TPD experiments, which is consistent with the XPS data in Figure 2 and rules out the possibility that the decrease in the area of the CO peak was due to agglomeration of the metal. The decrease in the CO peak area is, therefore, consistent with carbon buildup, which blocks active sites on the Co surface.

To study how oxidation of the supported cobalt affects its reactivity toward ethanol, TPD experiments were also performed with a Co/YSZ(100) sample that was predosed with O_2 and with

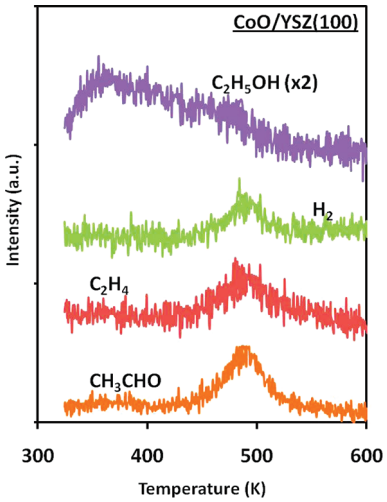

Figure 7. TPD spectra obtained from a CoO/YSZ(100) sample following a 2 L dose of C_2H_5OH at 300 K.

a CoO/YSZ(100) sample. TPD data obtained from a 1 ML Co/YSZ(100) sample that was exposed to 1 L of O_2 followed by 2 L of C_2H_5OH TPD at 300 K are shown in Figure 6, and the product relative yields are listed in Table 1. XPS analysis of Co/YSZ(100) samples exposed to similar amounts of O_2 indicated that the Co remained predominantly metallic after this treatment. Thus, the oxygen-dosed sample most likely contains only a surface layer of adsorbed oxygen on the cobalt.

The TPD results for this sample have some similarities to and some differences from those obtained from the sample that was not predosed with O_2 (see Figure 4b). The similarities include the net dehydration of ethanol, which occurs on the exposed portions of the YSZ(100) surface and produces C_2H_4 at 518 K, and decarbonylation of adsorbed ethoxide groups on the supported Co, which gives rise to the CO peak at 330 K. The primary differences are the selective oxidation of ethanol, producing acetaldehyde at 330 K and the appearance of a second CO peak at 518 K. As will be discussed below, this high-temperature CO product can be attributed to the oxidation of carbon atoms on the Co surface that were deposited via the decarbonylation pathway at lower temperature.

Ethanol TPD data obtained from a 1 ML Co/YSZ(100) sample that was oxidized by exposure to 1000 L of O_2 at 700 K is shown in Figure 7; the product relative yields are tabulated and listed in Table 1. As described above, this oxidation treatment produces a sample in which the cobalt is present primarily as CoO (i.e., Co^{2+}). In addition to a broad feature for molecular C_2H_5OH between 310 and 475 K, and a C_2H_4 peak at 480 K that can be attributed to reaction on exposed portions of the YSZ(100) surface, the only other carbon-containing product detected was CH_3CHO, which also desorbed at 480 K. Note that this peak temperature is 150 K higher than that observed for the O_2-dosed Co/YSZ(100) sample. The possible origin of this selective oxidation product will be discussed below.

DISCUSSION

As noted in the Introduction, the goals of this study were to determine both the active sites for the reaction of ethanol to acetaldehyde, which is thought to be a key step in the steam reforming of ethanol on supported Co catalysts, and the role that

dx.doi.org/10.1021/cs200404h |ACS Catal. 2011, 1, 1414–1420

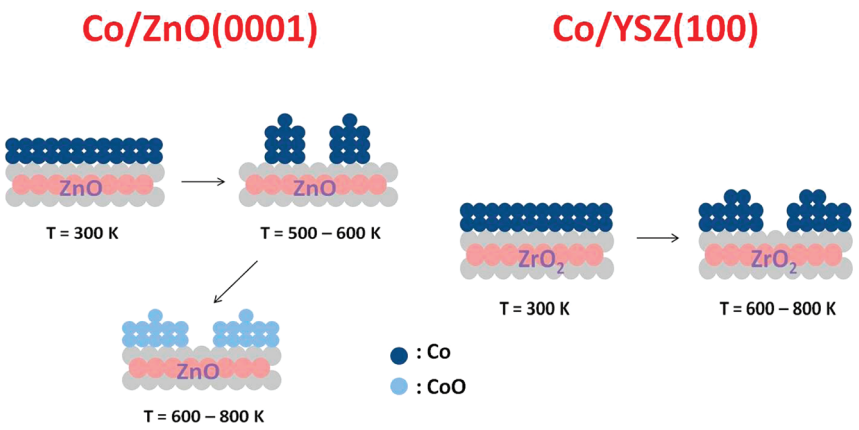

Figure 8. Schematic diagrams showing the structural evolution of vapor-deposited Co films on YSZ(100) and ZnO(0001).

the support plays in directing the overall catalyst reactivity. Insight into both of these issues can be obtained by comparing the results obtained in this study for model Co/YSZ(100) catalysts with those obtained in our previous studies of the reaction of ethanol on Co/ZnO(0001)[25] and polycrystalline Co foils.[24] Figure 8 shows schematically the structural evolution during the thermal annealing of Co films on both YSZ(100) and ZnO(0001). For both supports, the vapor-deposited Co forms two-dimensional island structures at 300 K. Although the Co film does undergo some agglomeration upon heating on both supports, it interacts much more strongly with YSZ(100), resulting in a relatively stable film, for temperatures up to 800 K. Although there was a strong interaction at the Co-YSZ(100) interface, the Co did not become oxidized via reaction with the support. This is in contrast to Co on ZnO(0001), for which significant agglomeration of the Co film occurred upon heating to only 600 K, indicating a relatively weak interaction at the Co−ZnO interface. These results are consistent with studies of high surface area supported Co catalysts, where it has also been observed that Co-support interactions vary significantly with the identity of the support and that Co/ZrO_2 catalysts are particularly stable.[13]

Despite the much weaker interaction of Co with ZnO(0001) relative to YSZ(100), Co reacts with oxygen on the ZnO(0001) surface between 700 and 800 K to from CoO particles, which then spread back across the surface. This result suggests that there is a much more facile exchange of oxygen between the Co and the ZnO support compared with the less reducible YSZ. As will be discussed below, this difference may affect the steady-state concentration of carbon on the Co during SRE on Co/ZrO_2 and Co/ZnO catalysts.

The primary reaction pathway for ethanol on YSZ(100) was net dehydration to produce ethylene at 485 K. This is in contrast to what has been reported for the reaction of ethoxy groups on ZnO(0001), where the primary pathway is dehydrogenation to produce acetaldehyde, which either desorbs or is further oxidized to acetate.[25,39] The net dehydration product, ethylene, is observed only as a minor product on the ZnO(0001) surface. Since ethylene is a potential coke precursor, the higher activity of the YSZ(100) surface for ethylene production may make Co/ZrO_2 catalysts more prone to coking than Co/ZnO.

The TPD results for metallic Co films on YSZ(100) are in agreement with our previous TPD studies of the reaction of ethanol on polycrystalline Co foils,[24] where it was concluded that a CO peak near 365 K resulted from decarbonylation of ethoxide

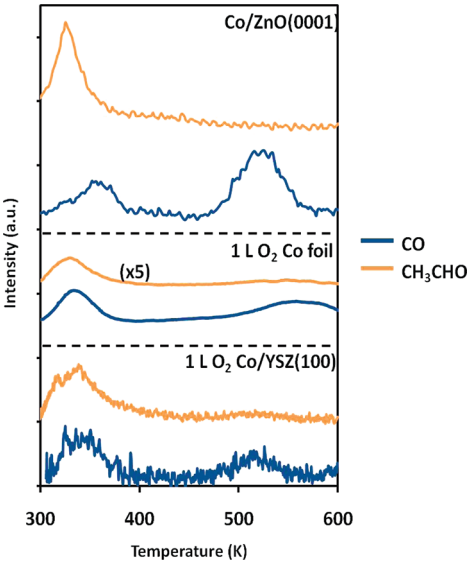

Figure 9. Comparison of CH_3CHO and CO spectra obtained following 2 L C_2H_5OH dose on (a) Co/ZnO(0001) (b) 1 L O_2 predosed polycrystalline Co foil, and (c) 1 L O_2 predosed Co/YSZ(100).

intermediates adsorbed on metallic Co sites. The methyl groups produced by this pathway remain on the surface and ultimately decompose to produce H_2 and adsorbed carbon. The data in Figures 4b and 7 demonstrates that this is also the case for Co/YSZ(100).

The ethanol TPD results obtained from the oxygen-dosed Co/YSZ(100) sample are more interesting, since they show the production of CH_3CHO, which is thought to be a key intermediate in the overall SRE reaction, at 330 K. For comparison purposes, the CO and CH_3CHO spectra obtained during ethanol TPD runs from the O_2-dosed Co/YSZ(100) sample, an O_2-dosed polycrystalline Co foil,[24] and Co/ZnO(0001)[25] are displayed in Figure 9. Note that the spectra from the O_2-dosed Co/YSZ(100) and Co foil samples are similar, with CH_3CHO being produced near 330 K, corresponding to an activation energy of only 86 kJ/mol determined using a Redhead analysis assuming first-order desorption with a prefactor of 10^{13} s^{-1}. Since XPS data for both samples show only metallic Co, the production of acetaldehyde can be attributed to abstraction of a hydrogen from an adsorbed ethoxide intermediate by an oxygen

dx.doi.org/10.1021/cs200404h |ACS Catal. 2011, 1, 1414–1420

atom adsorbed on a Co^0 site. The low-temperature CO peaks on both surfaces are indicative of the decarbonylation pathway that also proceeds on Co^0 sites, and the high-temperature CO peak results from oxidation of adsorbed carbon that is a byproduct of the decarbonylation reaction.

It is also noteworthy that the CH_3CHO and CO desorption curves in the ethanol TPD data from a 2 ML Co/ZnO(0001) sample without codosed O_2 (see Figure 9)[25] are similar to those obtained here for the O_2-dosed 1 ML Co/YSZ(100) sample, with CH_3CHO again being produced below 350 K. This suggests that the same reaction pathways occur on both samples. Since O_2 was not dosed on the Co/ZnO(0001) sample, the oxygen required for the dehydrogenation reaction that produces CH_3CHO at 325 K must be supplied by the ZnO(0001) support. The fact that the high-temperature CO peak at 518 K due to the carbon burnoff reaction is much larger for Co/ZnO(0001) compared with O_2-dosed Co/YSZ(100) is also consistent with facile transfer of oxygen from the ZnO to the Co. These results demonstrate that for Co/ZnO(0001), oxygen supplied by the reducible support can be used to remove carbon from the Co, but oxygen must be provided from the gas phase for this reaction to proceed on Co/YSZ(100).

This observation is similar to that reported by Song and Ozkan[17] in a study in which they compared ZrO_2 to CeO_2 as supports for cobalt SRE catalysts. Their steady-state kinetics measurements and XPS and microscopy analysis of the extent of carbon deposition showed Co/ZrO_2 to be much more prone to deactivation from carbon buildup compared with Co/CeO_2. They attributed this difference to the ability of the CeO_2 support to transfer oxygen to the Co, which could then be used to oxidize carbon deposits.

Although the selectivity for the production of acetaldehyde during ethanol TPD was nearly the same on the CoO/YSZ(100) and O_2-dosed Co/YSZ(100) samples (Table 1), the difference in temperatures at which acetaldehyde was produced indicates that CoO (or Co^{2+}) is much less reactive toward ethanol than metallic or oxygen-covered cobalt. For the CoO/YSZ(100) sample (Figure 7), the acetaldehyde product resulting from reaction on the CoO was produced at 480 K, which is 150 K higher than the acetaldehyde peak from the O_2-dosed Co/YSZ(100) sample. In our previous study, it was found that CoO particles on ZnO(0001) were even less reactive toward ethanol, with no products attributable to reaction on the CoO being observed during ethanol TPD experiments.[25] In that case, it is possible that a mixed Co−Zn oxide was formed, and this may have contributed to the lower reactivity. In any event, both of these studies demonstrate that oxygen-covered metallic cobalt is much more active for the dehydrogenation of ethoxide to produce acetaldehyde compared with CoO. This, in turn, argues against the ethoxide-to-acetaldehyde reaction occurring on Co^{2+} sites and is in agreement with previous studies[15,19,40] in which it has been concluded that Co^0 is required to obtain high SRE activity.

Although oxidized Co does not appear to provide the active sites for the dehydrogenation of ethoxide to produce acetaldehyde, the results of this study do suggest that adsorbed oxygen is required to obtain high activity for this reaction. Under actual SRE conditions, adsorbed OH or O atoms produced by dissociative adsorption of water on the metal may therefore be involved in this reaction. The results obtained from reducible supports such as ZnO[22] and CeO_2[18,41] suggest that for these supports, facile exchange of oxygen from the support to the metal may also play a role. Under SRE conditions, reoxidation of the support could occur by reaction with water. This bifunctional pathway is analogous to that which has been proposed for the water gas shift reaction on Pd/CeO_2 catalysts.[42] It may also be at least partially responsible for some of the support effects that have been reported for Co-based SRE catalysts.

CONCLUSIONS

The results of this study provide new insight into the active sites for the conversion of ethanol to acetaldehyde on supported Co ethanol steam reforming catalysts and the role of the support in determining overall reactivity. Both oxygen-covered metallic Co and CoO were found to be active for the dehydrogenation of adsorbed ethoxides to produce acetaldehyde, which is thought to be a key step in the overall SRE pathway. The activation energy for this reaction, however, was much lower on oxygen-modified metallic Co surfaces (86 kJ/mol) compared with CoO (126 kJ/mol). Comparisons of the results obtained for the Co/YSZ(100) and Co/ZnO(0001) model catalysts revealed large differences in the strength of the interaction of the Co with the support, which may affect catalyst stability. The transfer of oxygen from the support to the Co was also found to be much more facile on ZnO compared with ZrO_2. This process may be partially responsible for the reported higher activity of Co supported on reducible supports, such as ZnO and CeO_2, compared with more refractory supports, such as ZrO_2 and MgO.

AUTHOR INFORMATION

Corresponding Author

*E-mail: vohs@seas.upenn.edu.

ACKNOWLEDGMENT

Funding for this study was provided by the U.S. Department of Energy (Grant No. DE-FG02-04ER15605). We also thank Dr. Matthew Hyman for assistance in collecting some of the data for the Co foil.

REFERENCES

(1) Jacobson, M. Z.; Colella, W. G.; Golden, D. M. *Science* **2005**, *308*, 1901–1905.
(2) Wang, L.; Husar, A.; Zhou, T. H.; Liu, H. T. *Int. J. Hydrogen Energy* **2003**, *28*, 1263–1272.
(3) Haryanto, A.; Fernando, S.; Murali, N.; Adhikari, S. *Energy Fuels* **2005**, *19*, 2098–2106.
(4) Iwasa, N.; Takezawa, N. *Bull. Chem. Soc. Jpn.* **1991**, *64*, 2619–2623.
(5) Ni, M.; Leung, D. Y. C.; Leung, M. K. H. *Int. J. Hydrogen Energy* **2007**, *32*, 3238–3247.
(6) Benito, M.; Padilla, R.; Rodriguez, L.; Sanz, J. L.; Daza, L. *J. Power Sources* **2007**, *169*, 167–176.
(7) Marino, F. J.; Cerrella, E. G.; Duhalde, S.; Jobbagy, M.; Laborde, M. A. *Int. J. Hydrogen Energy* **1998**, *23*, 1095–1101.
(8) Llorca, J.; Homs, N.; Sales, J.; de la Piscina, P. R. *J. Catal.* **2002**, *209*, 306–317.
(9) Liguras, D. K.; Kondarides, D. I.; Verykios, X. E. *Appl. Catal. B* **2003**, *43*, 345–354.
(10) Rasko, J.; Hancz, A.; Erdohelyi, A. *Appl. Catal. A* **2004**, *269*, 13–25.
(11) Breen, J. P.; Burch, R.; Coleman, H. M. *Appl. Catal. B* **2002**, *39*, 65–74.

(12) Haga, F.; Nakajima, T.; Miya, H.; Mishima, S. *Catal. Lett.* **1997**, *48*, 223–227.
(13) Song, H.; Zhang, L. Z.; Watson, R. B.; Braden, D.; Ozkan, U. S. *Catal. Today* **2007**, *129*, 346–354.
(14) Lin, S. S. Y.; Kim, D. H.; Ha, S. Y. *Catal. Lett.* **2008**, *122*, 295–301.
(15) Karim, A. M.; Su, Y.; Engelhard, M. H.; King, D. L.; Wang, Y. *ACS Catal.* **2011**, *1*, 279–286.
(16) Sahoo, D. R.; Vajpai, S.; Patel, S.; Pant, K. K. *Chem. Eng. J.* **2007**, *125*, 139–147.
(17) Song, H.; Ozkan, U. S. *J. Catal.* **2009**, *261*, 66–74.
(18) Wang, H.; Ye, J. L.; Liu, Y.; Li, Y. D.; Qin, Y. N. *Catal. Today* **2007**, *129*, 305–312.
(19) Batista, M. S.; Santos, R. K. S.; Assaf, E. M.; Assaf, J. M.; Ticianelli, E. A. *J. Power Sources* **2003**, *124*, 99–103.
(20) Casanovas, A.; Roig, M.; de Leitenburg, C.; Trovarelli, A.; Llorca, J. *Int. J. Hydrogen Energy* **2010**, *35*, 7690–7698.
(21) Tuti, S.; Pepe, F. *Catal. Lett.* **2008**, *122*, 196–203.
(22) Llorca, J.; Dalmon, J. A.; de la Piscina, P. R.; Homs, N. *Appl. Catal. A* **2003**, *243*, 261–269.
(23) Hyman, M. P.; Martono, E.; Vohs, J. M. *J. Phys. Chem. C* **2010**, *114*, 16892–16899.
(24) Hyman, M. P.; Vohs, J. M. *Surf. Sci.* **2011**, *605*, 383–389.
(25) Martono, E.; Hyman, M. P.; Vohs, J. M. *Phys. Chem. Chem. Phys.* **2011**, *13*, 9880–9886.
(26) Padilla, R.; Benito, M.; Rodriguez, L.; Serrano, A.; Munoz, G.; Daza, L. *Int. J. Hydrogen Energy* **2010**, *35*, 8921–8928.
(27) Song, H.; Zhang, L. Z.; Ozkan, U. S. *Ind. Eng. Chem. Res.* **2010**, *49*, 8984–8989.
(28) Nishiguchi, T.; Matsumoto, T.; Kanai, H.; Utani, K.; Matsumura, Y.; Shen, W. J.; Imamura, S. *Appl. Catal. A* **2005**, *279*, 273–277.
(29) Ikonomov, J.; Stoychev, D.; Marinova, T. *Appl. Surf. Sci.* **2000**, *161*, 94–104.
(30) Kumar, L.; Sarma, D. D.; Krummacher, S. *Appl. Surf. Sci.* **1988**, *32*, 309–319.
(31) Bridge, M. E.; Lambert, R. M. *Surf. Sci.* **1979**, *82*, 413–424.
(32) Tan, B. J.; Klabunde, K. J.; Sherwood, P. M. A. *J. Am. Chem. Soc.* **1991**, *113*, 855–861.
(33) Dilara, P. A.; Petrie, W. T.; Vohs, J. M. *Appl. Surf. Sci.* **1997**, *115*, 243–251.
(34) Dilara, P. A.; Vohs, J. M. *J. Phys. Chem.* **1995**, *99*, 17259–17264.
(35) Dumont, J. A.; Mugumaoderha, M. C.; Ghijsen, J.; Thiess, S.; Drube, W.; Waz, B.; Tolkiehn, M.; Novikov, D.; de Groot, F. M. F.; Sporken, R. *J. Phys. Chem. C* **2011**, *115*, 7411–7418.
(36) Castro, G.; Hulse, J. E.; Kuppers, J.; Gonzalezelipe, A. R. *Surf. Sci.* **1982**, *117*, 621–628.
(37) Matsuyama, T.; Ignatiev, A. *Surf. Sci.* **1981**, *102*, 18–28.
(38) Dilara, P. A.; Vohs, J. M. *Surf. Sci.* **1994**, *321*, 8–18.
(39) Vohs, J. M.; Barteau, M. A. *Surf. Sci.* **1989**, *221*, 590–608.
(40) Lebarbier, V. M.; Karim, A. M.; Engelhard, M. H.; Wu, Y.; Xu, B.; Peterson, E. J.; Datye, A. K.; Wang, Y. *Chem. Sus. Chem.* **2011**, in press, doi: 10.1002/cssc.201100240.
(41) Song, H.; Bao, X. G.; Hadad, C. M.; Ozkan, U. S. *Catal. Lett.* **2011**, *141*, 43–54.
(42) Gorte, R. J.; Zhao, S. *Catal. Today* **2005**, *104*, 18–24.